

The quadrate is tall and slender, resembling the quadrates of *Archaeopteryx* and the enantiornithine *Gobipteryx* in that it is nearly one-quarter the length of the skull<sup>13</sup>. This bone also resembles that of *Archaeopteryx* in the strong rostro-caudal compression of its latero-distal corner<sup>13</sup>. Proximally, the quadrate has two well differentiated heads. The lateral head articulates with a squamosal-postorbital facet, whereas the medial head is dorso-caudally directed toward the braincase. The palatine is long and slender, lacking the jugal process and tetra-radiate aspect of non-avian theropod palatines<sup>13</sup>.

Study of the skull of *Shuvuuia* provides further evidence for the avian affinities of the Alvarezsauridae and emphasizes the highly specialized nature of this bizarre lineage: *Shuvuuia* displays a number of unusual cranial (as well as postcranial) characters and some characters that are restricted to Aves among dinosaurs. The configuration of the jugal and suspensorium of *Shuvuuia* (Fig. 1) suggests a capacity for intracranial kinesis<sup>12,15–17</sup> (for example, the elevation and depression of the rostrum). Without ventral squamosal and dorsal quadratojugal processes, the streptostylic quadrate would have been free to swing antero-posteriorly<sup>12,15–17</sup>. The lack of a connection between the jugal and postorbital would have freed the jugal to act as a strut between the quadrate and rostrum. Forces directed longitudinally from the quadrate would rotate the rostrum around a transverse axis at a flexion area just anterior to the orbit. A thinning of the jugal (bending zone) just caudal to its lacrimal contact and the loose connection between the frontals and the preorbital bones (nasals and prefrontals/ectethmoids) indicate that the snout may have moved as a unit like in prokinetic birds<sup>12,15–17</sup> (Fig. 1c). This interpretation is supported by the absence of a continuous naso-orbital septum. Prokinesis is usually regarded as the primitive avian type of kinesis derived from either akinetic or mesokinetic archosaurian skulls<sup>12,15–17</sup> and has been seen in several early birds<sup>18–20</sup>. The design of the skull of *Shuvuuia* suggests that some motion, probably prokinetic, was possible, supporting the theory that prokinesis was a primitive type of kinesis.

A cladistic analysis based on 90 characters (six of which are multistate) places the Alvarezsauridae as the sister taxon to all avians except for *Archaeopteryx* (Fig. 4; see Supplementary information for character list, data matrix, and node diagnoses). Cranial characters of *Shuvuuia* that are shared only with birds among dinosaurs include the absence of a postorbital-jugal contact, the movable joint (which is not sutured) between the quadratojugal and quadrate, the separate articulation of the quadrate with the braincase, and the disproportionately large foramen magnum relative to the occipital condyle. The skulls of *Shuvuuia*, *Archaeopteryx*, and other avians share characters that are absent in velociraptorine theropods, the outgroup selected for this cladistic analysis. These characters include the absence of a squamosal-quadratojugal contact and a coronoid in the mandible, and the presence of a triradiate palatine, a caudal tympanic recess confluent with the columellar recess, and unserrated tooth crowns.

It has been claimed that alvarezsaurids are either specialized ornithomimosaurs<sup>21,22</sup> or a different group of non-maniraptoran theropods<sup>23</sup>, although in neither case has a cladistic analysis been published. Our phylogenetic studies and independent cladistic analyses indicate that the few similarities between alvarezsaurids and non-maniraptoran coelurosaurians are the result of convergent evolution<sup>4,5,24–26</sup>. For example, the ornithomimosaur *Pelecanimimus* bears numerous tiny teeth, with unserrated crowns, that are restricted to the anterior part of the maxilla<sup>27</sup>, and ornithomimosaurs (as well as oviraptorosaurs and therizinosaurids among non-avian maniraptorans) lack a coronoid bone<sup>28</sup>. Furthermore, if the pre-orbital ossification of *Shuvuuia* is identified as a prefrontal, it is larger than that of most maniraptoran dinosaurs and more comparable in size to that of ornithomimosaurs<sup>29</sup>. However, placing alvarezsaurids outside Maniraptora would require homoplasy in an extensive number of maniraptoran, avian, and metornithine synapomorphies<sup>4,5,24–26</sup>. □

Received 10 September; accepted 26 November 1997.

- Dashzeveg, D. *et al.* Extraordinary preservation in a new vertebrate assemblage from the Late Cretaceous of Mongolia. *Nature* **374**, 446–449 (1995).
- Perle, A., Norell, M. A., Chiappe, L. M. & Clark, J. M. Flightless bird from the Cretaceous of Mongolia. *Nature* **362**, 623–626 (1993).
- Perle, A. *et al.* Skeletal morphology of *Mononykus olecranus* (Theropoda: Avialae) from the Late Cretaceous of Mongolia. *Am. Mus. Novit.* **3105**, 1–29 (1994).
- Chiappe, L. M., Norell, M. A. & Clark, J. M. Phylogenetic position of *Mononykus* from the Upper Cretaceous of the Gobi Desert. *Mem. Queens. Mus.* **39**, 557–582 (1996).
- Chiappe, L. M., Norell, M. A. & Clark, J. M. *Mononykus* and birds: methods and evidence. *Auk* **114**, 300–302 (1997).
- Jerzykiewicz, T. & Russell, D. A. Late Mesozoic stratigraphy and vertebrates from the Gobi Basin. *Cretac. Res.* **12**, 345–377 (1991).
- Chiappe, L. M. Late Cretaceous birds of southern South America: anatomy and systematics of Enantiornithes and *Patagopteryx deferrariisi*. *Münchener Geowiss. Ab. A* **30**, 203–244 (1996).
- Currie, P. J. New information on the anatomy and relationships of *Dromaeosaurus albertensis* (Dinosauria, Theropoda). *J. Vert. Paleontol.* **15**, 576–591 (1995).
- Weishampel, D. B., Dodson, P. & Osmólska, H. *The Dinosauria* (Univ. of California Press, Berkeley, 1990).
- Cracraft, J. The lacrimal-ectethmoid bone complex in birds: a single character analysis. *Am. Midl. Nat.* **80**, 316–359 (1968).
- Romer, A. S. *Osteology of the Reptiles* (Univ. Chicago Press, 1956).
- Zusi, R. L. In *The Skull* Vol. 2 (eds Hanken, J. & Hall, B. L.) 391–437 (Univ. Chicago Press, 1993).
- Elzanowski, A. & Wellnhofer, P. Cranial morphology of *Archaeopteryx*: evidence from the seventh skeleton. *J. Vert. Paleontol.* **16**, 81–94 (1996).
- Sanz, J. L. *et al.* A nesting bird from the Early Cretaceous of Spain: implications for avian skull and neck evolution. *Science* **276**, 1543–1546 (1997).
- Zusi, R. L. A functional and evolutionary analysis of rhynchokinesis in birds. *Smithson. Contr. Zool.* **395**, 1–40 (1985).
- Simonetta, A. M. On the mechanical implications of the avian skull and their bearing on the evolution and classification of birds. *Q. Rev. Biol.* **35**, 206–220 (1960).
- Bock, W. J. Kinetics of the avian skull. *J. Morphol.* **114**, 1–42 (1964).
- Bühler, P. In *The Beginnings of Birds* (eds Hecht, M. K., Ostrom, J. H., Viohl, G. & Wellnhofer, P.) 135–140 (Proc. Int. Archaeopteryx Conf., Eichstätt, 1985).
- Hou, L., Martin, L. D., Zhou, Z. & Feduccia, A. Early adaptive radiation of birds: evidence from fossils from northeastern China. *Science* **274**, 1164–1167 (1996).
- Bühler, P., Martin, L. D. & Witmer, L. M. Cranial kinesis in the Late Cretaceous birds *Hesperornis* and *Parahesperornis*. *Auk* **105**, 111–122 (1988).
- Martin, L. D. & Rinaldi, C. How to tell a bird from a dinosaur. *Maps Digest* **17**, 190–196 (1994).
- Feduccia, A. *The Origin and Evolution of Birds* (Yale Univ. Press, New Haven, 1996).
- Sereno, P. The origin and evolution of dinosaurs. *Ann. Rev. Earth Planet. Sci.* **25**, 435–489 (1997).
- Novas, F. E. Alvarezsauridae, Cretaceous maniraptorans from Patagonia and Mongolia. *Mem. Queens. Mus.* **39**, 675–702 (1996).
- Novas, F. E. Anatomy of *Patagonykus puertai* (Theropoda, Maniraptora, Alvarezsauridae) from the Late Cretaceous of Patagonia. *J. Vert. Paleontol.* **17**, 137–166 (1997).
- Forster, C. A., Chiappe, L. M., Krause, D. W. & Sampson, S. D. The first Cretaceous bird from Madagascar. *Nature* **382**, 532–534 (1996).
- Pérez-Moreno, B. P. *et al.* A unique multitoothed ornithomimosaur from the Lower Cretaceous of Spain. *Nature* **370**, 363–367 (1994).
- Clark, J. M., Perle, A. & Norell, M. A. The skull of *Erlicosaurus andrewsi*, a Late Cretaceous “Segnosaur” (Theropoda: Therizinosauridae) from Mongolia. *Am. Mus. Novit.* **3115**, 1–39 (1994).
- Osmólska, H., Roniewicz, E. & Barsbold, R. A new dinosaur, *Gallimimus bullatus* n. gen. n. sp. (Ornithomimidae) from the Upper Cretaceous of Mongolia. *Palaentol. Pol.* **27**, 103–143 (1972).

Supplementary information is available on Nature's World-Wide Web site (<http://www.nature.com>) or as paper copy from Mary Sheehan at the London editorial office of Nature.

**Acknowledgements.** We thank A. Davidson and M. Ellison for the preparation and illustration of the specimens, respectively, and A. Milner, L. Witmer, G. Zweers, and J. Vanden Berge for useful reviews and discussions. The Chapman and Frick Memorial Funds of the AMNH and the National Science Foundation provided support for this research.

## Common reference frame for neural coding of translational and rotational optic flow

D. R. W. Wylie, W. F. Bischof & B. J. Frost\*

Department of Psychology, University of Alberta, Edmonton, Alberta T6G 2E9, Canada

\* Department of Psychology, Queen's University, Kingston, Ontario K7L 3N6, Canada

Self-movement of an organism through the environment is guided jointly by information provided by the vestibular system and by visual pathways that are specialized for detecting 'optic flow'<sup>1,2</sup>. Motion of any object through space, including the self-motion of organisms, can be described with reference to six degrees of freedom: rotation about three orthogonal axes, and translation along these axes. Here we describe neurons in the pigeon brain that respond best to optic flow resulting from

translation along one of the three orthogonal axes. We show that these translational optic flow neurons, like rotational optic flow neurons<sup>3-5</sup>, share a common spatial frame of reference with the semicircular canals of the vestibular system. The three axes to which these neurons respond best are the vertical axis and two horizontal axes orientated at 45° to either side of the body midline.

As the environment contains many stationary objects and surfaces, self-motion induces distinctive patterns of visual motion ('optic flow' or 'flowfields') across the entire retina<sup>6</sup>. Psychophysical research has illustrated the importance of optic flow for the control of posture and locomotion<sup>7,8</sup> and for the perception of self-motion<sup>9</sup>. Figure 1b, c shows flowfields resulting from both self-translation (Fig. 1c) and self-rotation (Fig. 1b). The shaded areas in Fig. 1c indicate differences in local motion in the translational flowfield. At one 'pole' in the direction of translation, flow radiates outward from the focus of expansion, while converging to the focus of contraction (not shown) behind the bird's head, with laminar at the 'equator'. In this figure, the bird is translating forward, along the z-axis. As the pigeon has laterally placed eyes, forward translation results in backward (that is, nasal to temporal) visual motion throughout much of the visual field of both eyes.

Neurons sensitive to translational and rotational optic flow have been found in the visual neuropile of the blowfly<sup>10</sup> and, in vertebrates, in extrastriate visual cortex<sup>11,12</sup>, the accessory optic system (AOS) and the vestibulocerebellum<sup>3-5,13</sup>. In pigeons, the AOS<sup>14</sup> and the vestibulocerebellum<sup>13</sup> contain neurons that are responsive to either translational or rotational flowfields. Here we show that the translation-sensitive neurons respond best to translational optic flow along one of three axes, namely, the vertical axis (y-axis) or one of two horizontal axes orientated at 45° to the midline.

We recorded the activity of neurons in the nucleus of the basal optic root (nBOR, a component of the AOS) and of Purkinje cells (complex spikes) in the ventral uvula and nodulus of the vestibulocerebellum in anaesthetized pigeons. Cells in these structures have large binocular receptive fields, covering much of the entire visual field of both eyes, and respond best to large moving visual stimuli that approximate to translational flowfields<sup>13,14</sup>. (Cells in the flocculus

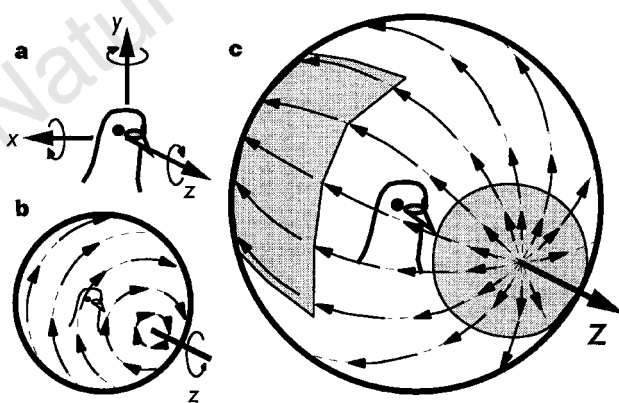


**Figure 1** Generic description for motion of an object in three-dimensional space and optic flowfields generated by translation along, and rotation about the z-axis. **a**, The generic description for motion of an object in three-dimensional space using the standard coordinate system. Motion can be described using a reference frame consisting of three orthogonal axes (x, y and z), and six degrees of freedom, three of translation (straight arrows) and three of rotation (curved arrows). This is an egocentric coordinate system, that is, it refers to motion of the bird. **b**, The optic flowfield resulting from a clockwise rotation of the bird about the z-axis. **c**, The optic flowfield resulting from translation (out from the page) along the z-axis. The shaded areas in **c** highlight the differences in local image motion at the 'pole' and 'equator' of the translational flowfield.

of the vestibulocerebellum selectively respond to rotational flowfields<sup>5,13</sup>.) The binocular neurons in the nBOR represent a small subpopulation: most nBOR neurons are monocular and were not studied here. We projected a translational flowfield onto the walls, ceiling and floor of the room with a specially designed 'translator'. The translator is similar to the 'planetarium projector'<sup>3,4</sup>

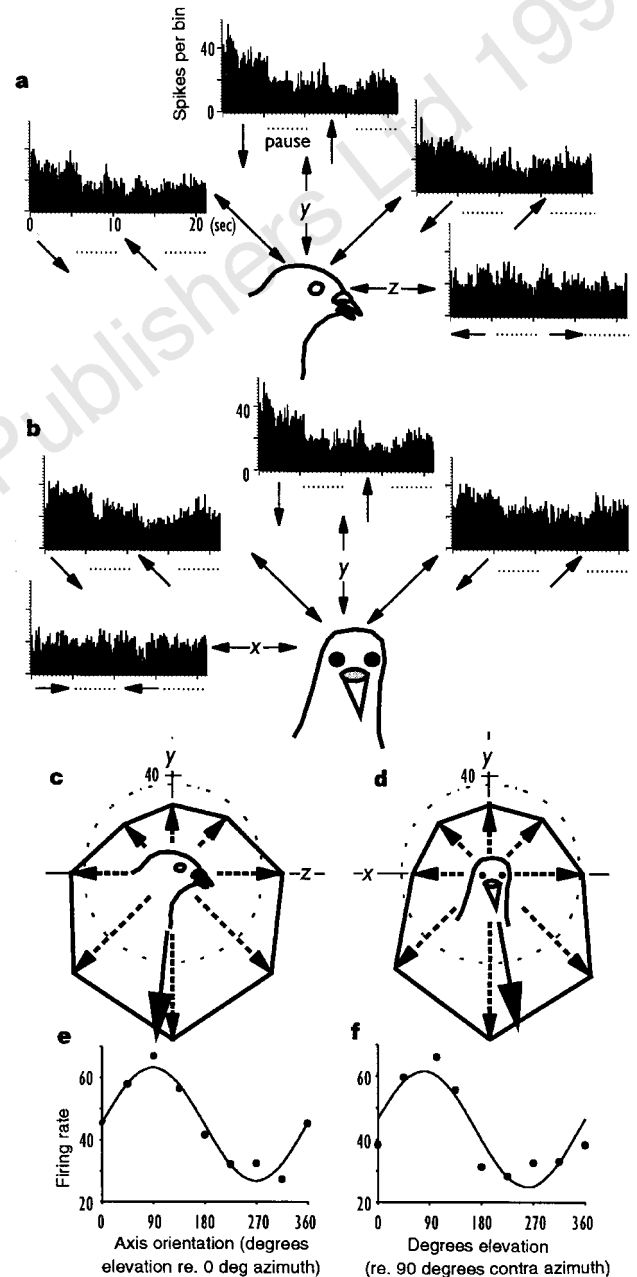


**Figure 2** Tuning curves of a binocular nBOR neuron that is maximally responsive to translational optic flow along the vertical axis are shown. **a, b**, PSTHs show the responses to translation along axes in the sagittal (**a**) and frontal (**b**) planes. The tuning curves are shown as polar plots for the sagittal and frontal planes in **c** and **d**, respectively, where firing rate (spikes per second) is plotted as a function of the orientation of the direction of translational flow. The orientation of an arrow reflects the orientation of the axis of the translator, and the arrowhead points in the direction in which the bird would be moving to produce such a flowfield. The broken circles represent the spontaneous firing rate, and the solid arrows indicate the best axes as determined from the best cosine fits. **e** and **f** show the best cosine fits to the tuning curves shown in **c** and **d**, respectively.

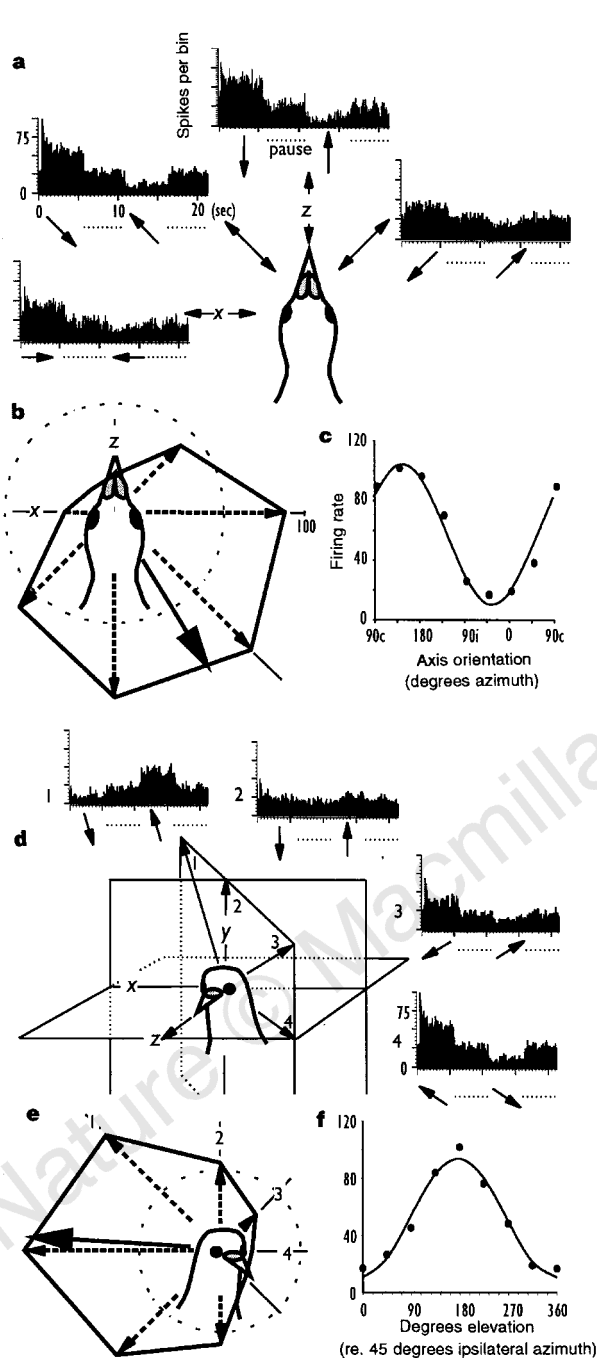


**Figure 3** Tuning curves of a binocular nBOR neuron that is maximally responsive to translational optic flow along an horizontal axis orientated  $\sim 45^\circ$  to the midline are shown. **a**, PSTHs show the responses of neurons to translation along axes in the horizontal plane. **d**, PSTHs show the responses to translation along axes in a vertical plane that intersects the horizontal plane at  $45^\circ$  ipsilateral azimuth. Polar plots of the tuning curves are shown in **b** and **e**, for the planes depicted in **a** and **d**, respectively. The broken circles represent the spontaneous firing rate, and the solid arrows indicate the best axis as determined from the best cosine fit. **c**, **f**, Show the best cosine fits to the tuning functions shown in **b** and **e**, respectively.  $90i$ ,  $90^\circ$  ipsilateral azimuth;  $90c$ ,  $90^\circ$  contralateral azimuth.

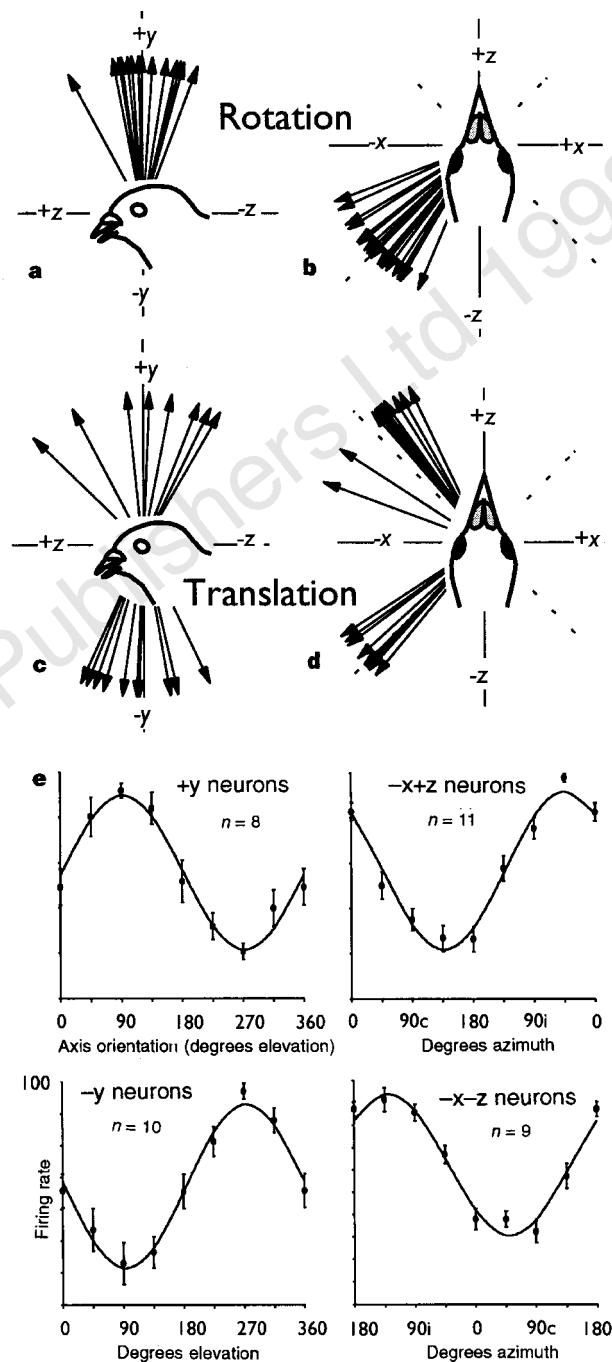


**Figure 4** Best axes of translation- and rotation-sensitive neurons in the vestibulocerebellum of pigeons. **a**, **b**, The reference frame of rotation-sensitive neurons in the flocculus (from ref. 5). **c**, **d**, The reference frame of the translation-sensitive neurons in the ventral uvula and nodulus. In **a**, **b**, each arrow represents the best axis about which a rotational visual flowfield resulted in maximal modulation. The arrows in **c**, **d**, represent the best axes of the translation-sensitive neurons in the uvula and nodulus from the present study. In **a**, **c**, the best axes are projected onto a sagittal plane and were determined from elevation tuning curves in that plane. Likewise, in **b**, **d**, the best axes are projected onto the horizontal plane and were determined from azimuthal tuning curves in that plane. **e**, The best cosine fits to the mean normalized tuning curves<sup>13</sup> for each of the four groups of translation-sensitive neurons are shown. For these curves, the firing rate in response to translation in each direction is expressed as a percentage of the cell's maximal firing rate, then averaged within groups. Average firing rate ( $\pm$ s.e.m.) is plotted as a function of the direction of translation.

in that it presents motion to the entire visual field, but is different in that it simulates translations rather than rotations (see Methods).

We found that although neurons were broadly tuned, they responded best to translational optic flow along a particular axis, but responded minimally to translation along axes orthogonal to this 'best axis'. Along the best axis, motion in one direction resulted in strong excitation, whereas motion in the opposite direction produced inhibition. We recorded data from 67 neurons that responded optimally to translational optic flow (38 neurons in the ventral uvula and nodulus of the vestibulocerebellum and 29 neurons in the nBOR). For simplicity, we describe the data as if all recordings were obtained from the left side of the brain.

Figure 2 shows the responses of an nBOR neuron to translational flowfields along several axes. In response to movement of a large handheld stimulus in the central part of the visual field (see Methods), this neuron was excited in response to upward visual flow in both hemifields but was insensitive to horizontal motion. Figure 2a, b shows peristimulus time histograms (PSTHs) illustrating the responses to translational optic flow in eight directions (45° apart) in both the sagittal (Fig. 2a) and the frontal (Fig. 2b) planes. The data from Fig. 2a, b are shown in Fig. 2c, d, where the average firing rate is plotted (in polar plots) as a function of the direction of translational optic flow. The orientation of an arrow reflects the orientation of the axis of the translator, and the arrowhead points in the direction in which the animal would be moving to produce such a flowfield. That is, the arrowhead points toward the focus of expansion in the flowfield. The solid arrows in the polar plots denote the 'best axis' for the tuning curves in Fig. 2c, d, determined from the best cosine fits shown in Fig. 2e, f. The fits are excellent, indicating that, for the two planes tested, the response magnitude of this neuron to translation in any direction  $\mathbf{d}$  was linearly related to the projection of  $\mathbf{d}$  onto the neuron's preferred direction. This neuron responded best to  $-y$  translation and was strongly inhibited by  $+y$  translation. Translational optic flow along the  $x$ -axis (Fig. 2b, d) and  $z$ -axis (Fig. 2a, c) produced very little modulation.

In contrast, the nBOR neuron shown in Fig. 3 showed little modulation to translation along the  $y$ -axis, but responded best to translational optic flow along a horizontal axis orientated at 45° ipsilateral azimuth. This neuron was excited by forward (temporal to nasal) movement of the handheld stimulus in the central region of both hemifields but was insensitive to vertical visual flow. Figure 3a shows PSTHs illustrating the responses to translation along eight directions in the horizontal plane (azimuthal tuning curve), whereas Fig. 3d shows PSTHs illustrating the responses to translation in eight directions in the vertical plane orthogonal to the horizontal plane and intersecting it at 45° ipsilateral azimuth (that is, the plane normal to the vector  $+x+z$ ). Polar plots are shown in Fig. 3b, e. This neuron was maximally modulated by translation along the horizontal axis orientated at ~45° ipsilateral azimuth, but showed little modulation to translation along orthogonal axes. Translation in the direction producing a focus of expansion 135° ipsilateral azimuth produced maximal excitation whereas the opposite direction produced maximal inhibition. Using the coordinate system shown in Fig. 1a, the best axis is approximately  $+x-z$ .

In the vestibulocerebellum, neurons responded best to translational flow along one of three roughly orthogonal axes. Eighteen neurons responded best to translation along the  $y$ -axis. Of these, eight were classified as  $+y$  neurons, and ten were classified as  $-y$  neurons. The best axes of these eighteen neurons, obtained from tuning curves in the sagittal plane, are shown in Fig. 4c.

Twenty vestibulocerebellar neurons responded best to translation along horizontal axes and showed minimal modulation in response to translation along the vertical axis. Of these neurons, nine were classified as  $-x-z$  neurons, as they were maximally excited by a flowfield with a focus of expansion at 135° ipsilateral azimuth. The other 11 neurons were maximally excited in response to a flowfield with a focus of expansion at 45° ipsilateral azimuth (they were

classified as  $-x+z$  neurons). The best axes of these 20 neurons, obtained from azimuthal tuning curves in the horizontal plane, are shown in Fig. 4d. Figure 4e shows the best cosine fits to the mean normalized tuning curves<sup>13</sup> for the four groups shown in Fig. 4c, d, where the average firing rate for each direction is expressed as a percentage of the cells' maximal firing rates. As in the case of the nBOR cells in Figs 2 and 3, the cosine fits are excellent, indicating that, for the planes tested, the response magnitude of these neurons to translation in any direction  $\mathbf{d}$  was linearly related to the projection of  $\mathbf{d}$  onto the neurons' preferred direction. Further, the cosine fits in Fig. 4e also show a phase shift of 90° between the  $-x-z$  and  $-x+z$  neurons, supporting the conclusion that the axes of the coordinate system are indeed orthogonal.

Our results indicate that the neural systems responsive to translational optic flow may be organized according to a spatial frame of reference consisting of three orthogonal axes: neurons respond best to translational optic flow along either the vertical axis ( $y$ -axis) or one of two horizontal axes orientated at 45° to the midline. It has been shown<sup>3-5</sup> (Fig. 4a, b) that this is the spatial frame of reference for the neural systems that are responsive to rotational optic flow. The vestibular semicircular canals share this same spatial frame of reference<sup>3,4</sup>, and the otolithic organs of the inner ear may also be organized according to this reference frame<sup>15,16</sup>.

Therefore, the neural systems, both visual and vestibular, responsible for the encoding of self-motion may be organized in a common reference frame with six degrees of freedom, three translational and three rotational. It has been argued that the three-axis system consisting of a vertical axis and two horizontal axes orientated 45° to the midline is the most economical<sup>17</sup>, and we suggest that there are neural computational advantages of a single spatial frame of reference is used. Indeed, this is the case in other multimodal sensorimotor systems<sup>18-21</sup>. □

#### Methods

Anaesthesia, surgery, and extracellular recording procedures have been described<sup>13,14</sup>. The translational optic flowfield stimulus was produced using a 'translator' projector suspended ~10 cm above the bird's head. The translator consisted of a hollow metal sphere (with a diameter of 8 cm), the surface of which was drilled with numerous small holes. A filament light source was moved along a segment of a diameter path within the sphere, so that a moving pattern of light dots was projected through the holes in the sphere's surface onto the walls, ceiling and floor of the room. Using gimbals, the axis of the spherical translational flowfield could be positioned to any orientation within three-dimensional space. The speed of the 'equatorial' dots was 1–2° per sec. For each sweep there was 5.3-s translation in one direction, followed by a 5.3-s pause, 5.3-s translation in the opposite direction, and a 5.3-s pause. PSTHs were summed from 5–10 sweeps using Spike2 software (Cambridge Electronic Designs).

Initially, once a cell was isolated, a large (~90° × 90°) handheld stimulus of random dots and lines was moved in various directions in the central areas of both visual fields. With this stimulus, neurons responded best to either vertical or horizontal motion in both hemifields. Next, using the translator, the responses of neurons to translational optic flow along the  $x$ ,  $y$  and  $z$  axes were recorded. After this, tuning curves were determined by presenting translation along various axes (of 45° apart) in a particular plane. For neurons that preferred horizontal translation, azimuthal tuning curves were obtained for the horizontal plane and then elevation tuning curves were obtained for the vertical plane that intersected the horizontal plane along the axis that produced maximal modulation (Fig. 3). For neurons that preferred vertical translation, elevation tuning curves were obtained for first the sagittal plane and then the frontal plane (Fig. 2). Least-square fits of cosines to each tuning curve were obtained and the maximum was denoted as the 'best axis', within the plane of the tuning curve.

Received 7 July; accepted 22 December 1997.

1. Simpson, J. I. The accessory optic system. *Annu. Rev. Neurosci.* 7, 13–41 (1984).
2. Frost, B. J., Wylie, D. R. & Wang, Y.-C. in *Perception and Motor Control in Birds* (eds Green, P. & Davies, M.) 249–266 (Springer, Berlin, 1994).

3. Simpson, J. I., Graf, W. & Leonard, C. in *Progress in Oculomotor Research* (eds Fuchs, A. F. & Becker, W.) 475–484 (Elsevier, Amsterdam, 1981).
4. Graf, W., Simpson, J. I. & Leonard, C. S. Spatial organization of visual messages of the rabbit's cerebellar flocculus. II. Complex and simple spike responses of Purkinje cells. *J. Neurophysiol.* **60**, 2091–2121 (1988).
5. Wylie, D. R. & Frost, B. J. Responses of pigeon vestibulocerebellar neurons to optokinetic stimulation: II. The 3-dimensional reference frame of rotation neurons in the flocculus. *J. Neurophysiol.* **70**, 2647–2659 (1993).
6. Gibson, J. J. The visual perception of objective motion and subjective movement. *Psychol. Rev.* **61**, 304–314 (1954).
7. Lee, D. N. & Aronson, E. Visual proprioceptive control of standing in human infants. *Percept. Psychophys.* **15**, 529–532 (1974).
8. Owen, D. H. in *Perception & Control of Self-Motion* (eds Warren, R. & Fuchs, A. F.) 289–322 (Lawrence Erlbaum, Hillsdale, New Jersey, 1990).
9. Anderson, G. J. Perception of self-motion: psychophysical and computational approaches. *Psychol. Bull.* **99**, 52–65 (1986).
10. Krapp, H. G. & Hengstenberg, R. Estimation of self-motion by optic flow processing in single visual interneurons. *Nature* **384**, 463–466 (1996).
11. Duffy, C. J. & Wurtz, R. H. Sensitivity of MST neurons to optic flow stimuli. I. A continuum of response selectivity to large-field stimuli. *J. Neurophysiol.* **65**, 1329–1345 (1991).
12. Bradley, D. C., Maxwell, M., Anderson, R. A. & Banks, M. S. Mechanisms of heading perception in primate visual cortex. *Science* **273**, 1544–1547 (1996).
13. Wylie, D. R., Kripalani, T.-K. & Frost, B. J. Responses of pigeon vestibulocerebellar neurons to optokinetic stimulation: I. Functional organization of neurons discriminating between translational and rotational visual flow. *J. Neurophysiol.* **70**, 2632–2646 (1993).
14. Wylie, D. R. & Frost, B. J. Binocular neurons in the nucleus of the basal optic root (nBOR) of the pigeon are selective for either translational or rotational visual flow. *Vis. Neurosci.* **5**, 489–495 (1990).
15. Hess, B. J. & Dieringer, N. Spatial organization of linear vestibuloocular reflexes of the rat: responses during horizontal and vertical linear acceleration. *J. Neurophysiol.* **66**, 1805–1818 (1991).
16. Macpherson, J. M. Strategies that simplify the control of quadrupedal stance. I. Forces at the ground. *J. Neurophysiol.* **60**, 204–217 (1988).
17. Simpson, J. I. & Graf, W. in *Adaptive Mechanisms in Gaze Control: Facts and Theories* (eds Berthoz, A. & Melvill-Jones, G.) 3–16 (Elsevier, Amsterdam, 1985).
18. Soechting, J. F. & Flanders, M. Moving in three-dimensional space: frames of reference, vectors, and coordinate systems. *Annu. Rev. Neurosci.* **15**, 167–191 (1992).
19. Knudsen, E. I., du Lac, S. & Esterly, S. D. Computational maps in the brain. *Annu. Rev. Neurosci.* **10**, 41–65 (1987).
20. Jay, M. F. & Sparks, D. L. Auditory receptive fields in primate superior colliculus shift with changes in eye position. *Nature* **309**, 345–347 (1984).
21. Masino, T. & Knudsen, E. I. Horizontal and vertical components of head movement are controlled by distinct neural circuits in the barn owl. *Nature* **345**, 434–437 (1990).

**Acknowledgements.** We thank M. Dawson, D. Crewther and I. Curthoys for comments on this manuscript, and K. Lau and R. Glover for technical assistance. This research was supported by grants from the NSERC and AHFMR (to D.R.W.W.).

Correspondence and requests for material should be addressed to D.R.W.W. (e-mail: dwylie@psych.ualberta.ca).

## Sniffing and smelling: separate subsystems in the human olfactory cortex

N. Sobel\*, V. Prabhakaran\*, J. E. Desmond†, G. H. Glover‡, R. L. Goode§, E. V. Sullivan\*|| & J. D. E. Gabrieli\*†

\* Program in Neuroscience and Departments of † Psychology, ‡ Radiology, § ENT Surgery and || Psychiatry & Behavioral Sciences, Stanford University, Stanford, California 94305, USA  
§ Palo Alto VA Hospital, Palo Alto, California 94305, USA

The sensation and perception of smell (olfaction) are largely dependent on sniffing, which is an active stage of stimulus transport and therefore an integral component of mammalian olfaction<sup>1,2</sup>. Electrophysiological data obtained from study of the hedgehog, rat, rabbit, dog and monkey indicate that sniffing (whether or not an odorant is present) induces an oscillation of activity in the olfactory bulb, driving the piriform cortex in the temporal lobe, in other words, the piriform is driven by the olfactory bulb at the frequency of sniffing<sup>3–6</sup>. Here we use functional magnetic resonance imaging (fMRI) that is dependent on the level of oxygen in the blood to determine whether sniffing can induce activation in the piriform of humans, and whether this activation can be differentiated from activation induced by an odorant. We find that sniffing, whether odorant is present or

absent, induces activation primarily in the piriform cortex of the temporal lobe and in the medial and posterior orbito-frontal gyri of the frontal lobe. The source of the sniff-induced activation is the somatosensory stimulation that is induced by air flow through the nostrils. In contrast, a smell, regardless of sniffing, induces activation mainly in the lateral and anterior orbito-frontal gyri of the frontal lobe. The dissociation between regions activated by olfactory exploration (sniffing) and regions activated by olfactory content (smell) shows a distinction in brain organization in terms of human olfaction.

The brains of six subjects were scanned in an experiment that contrasted the sniffing of non-odorized clean air with lack of sniffing. Sniffing induced activation primarily in the ventral temporal region (piriform, entorhinal and parahippocampal regions) and also in a small portion of the posterior and medial orbito-frontal cortex in all six subjects (Fig. 1a). Four subjects were then each rescanned four times; in each scan each subject was sniffing continuously at a different sniff-rate. Sniff-rate consistently determined the frequency of activity in the piriform cortex in all 16 scans (Fig. 2). Including the control experiments described below, sniff-induced activation occurred in the piriform of all 13 subjects tested. In 11 of the 13 subjects, sniff-induced activation was greater in the left piriform than in the right piriform (85% of subjects,  $P < 0.02$ ).

In six additional experiments, we asked which sniffing-associated factor caused the piriform activation. First, we asked whether the sniff-induced activation was related to the motor action of sniffing or to the somatosensory stimulation induced by sniffing. Four subjects were scanned while they were sniffing with their nostrils blocked (that is, they were unsuccessfully trying to sniff); this eliminated the somatosensory stimulation associated with sniffing but maintained the motor element of sniffing. Such attempts to sniff did not induce significant activation in the piriform in any of the four subjects (Fig. 3B, d).

The same four subjects were then scanned under conditions of artificial sniffing, in which non-odorized air was puffed into the nostrils at a flow, duration, and rate similar to that of a natural sniff. This procedure, which eliminated the motor action but maintained the somatosensory element of sniffing, induced significant activation in the piriform of all four subjects (Fig. 3B, c).

An additional subject was scanned three times while sniffing with a partial occlusion of the nostrils that left 2-, 4-, or 6-mm opening. The smaller opening was associated with increased motor effort and decreased flow, whereas the larger opening was associated with decreased motor effort and increased flow. An increase in unoccluded-nostril diameter was consistently accompanied by an increase of activation in the piriform; in other words activation was related to the somatosensory sensation of air flow.

To address the possibility that sniff-induced activation may have reflected an fMRI contrast artefact (because of the periodic change in air content surrounding the nasal passages), rather than brain activity, we tested four additional subjects while they were sniffing before and after applying a topical anaesthetic to the nasal passages. Subjects were given an anaesthetic combined with a nasal dilator which, taken together, increased air flow as measured by anterior rhinometry. If sniff-induced activation were an artefact of air flow, this procedure would increase sniff-induced activation. Three of the four subjects reported a slight numbing sensation in the nostrils (but see ref. 7). The anaesthesia markedly reduced sniff-induced activation in the three subjects who reported a reduction in sensation (compare Fig. 3Ba, b), but not in the subject who did not report a reduction in sensation. The anaesthesia did not affect the perception of odours by these subjects in a standard test of olfactory identification (The University of Pennsylvania Smell Identification Test)<sup>8</sup>. Thus, sniff-induced activation is not an artefact related to air flow, but is instead related to brain activity induced by the sensation of air flow.

To address further the issue of possible airflow artefacts, we